Novel scintillator-based x-ray spectrometer for use on high repetition laser plasma interaction experiments

D. R. Rusby,[1,2,a)] C. D. Armstrong,[1,2] C. M. Brenner,[1] R. J. Clarke,[1] P. McKenna,[2] and D. Neely[1,2]
[1]*STFC, Rutherford Appleton Laboratory, Chilton, Didcot OX11 0QX, United Kingdom*
[2]*SUPA, Department of Physics, University of Strathclyde, Glasgow G4 0NG, United Kingdom*

(Received 12 December 2017; accepted 2 June 2018; published online 6 July 2018)

The characterisation of x-rays from laser-plasma interactions is of utmost importance as they can be useful for both monitoring electron dynamics and also applications in an industrial capacity. A novel versatile scintillator x-ray spectrometer diagnostic that is capable of single shot measurements of x-rays produced from laser-plasma interactions is presented here. Examples of the design and extraction of the temperature of the spectrum of x-rays produced in an intense laser-solid interaction (479 ± 39 keV) and the critical energy from a betatron source (30 ± 10 keV) are discussed. Finally, a simple optimisation process involving adjusting the scintillator thickness for a particular range of input spectra is demonstrated.
https://doi.org/10.1063/1.5019213

I. INTRODUCTION

When a high-intensity laser ($>1 \times 10^{18}$ W/cm^2) interacts with an underdense or overdense plasma, a relativistic population of electrons is generated. These electrons can create x-rays that have a short pulse duration and small source size and are highly penetrating due to their energy spectrum. X-rays produced from laser-plasma interactions are of great interest for radiography applications[1] and as a method for determining the internal hot-electron temperatures and flux from solid target experiments.[5–7] One of the simplest techniques for observing the x-ray spectrum is to use an absorption based spectrometer.[5,8] These spectrometers usually use high density filters to attenuate x-rays of energy greater than hundreds of keV, which are readily achievable from many high-power laser-solid interactions.[3,4,12] Such diagnostics are widely used because of the ability to determine the response curves to x-rays with ease using Monte Carlo simulations, such as GEANT4, that contains the relevant photon attenuation and absorption physics.[9–11] Many current absorption spectrometers rely on the film as the detector material, most commonly the FUJI-film image plate,[5,8] as it is highly sensitive, versatile, and resistant to any electromagnetic pulse effects that are present during high-powered laser interactions.[13] However, one of the main limitations is that the processing time required for the image plate is not in line with the new laser systems being developed that promise faster repetition; therefore, the development of spectrometers capable of operating at higher repetition rates is required.

A spectrometer that can operate at repetition rates up to 10 Hz[14] would require a novel method of detection and x-ray attenuation to provide good spectral resolution. Scintillators are materials that absorb a high-energy photon which excites/ionises an electron through the photoelectric effect. This ionised electron transfers energy to other surrounding electrons, exciting them to higher energy levels within their structure. Finally, the scintillation decay of the excited electrons within the atoms can emit light in the visible spectrum allowing it to be easily recorded.

The decay times of the energy states vary depending on the chosen scintillator, typically from hundreds of nanoseconds to sub-nanoseconds. Current ultra high-power laser systems operate with a repetition rate ranging from anything as low as 10^{-4} to 10's Hz; in the future, this is only expected to get quicker as laser technology develops. As the decay times of scintillators are much shorter than the repetition rate, they will be ideally suited to the current state-of-the-art and future laser systems.

To provide the necessary attenuation to monitor the highest energy of x-rays, filtering would normally be put in-front of the active material. However, the scintillators can be used simultaneously as both the attenuator and the detection media. In this paper, we will discuss the use of a 1D array of scintillators as an x-ray spectrometer and some results obtained with this arrangement.[2] This keeps the aperture and overall size of the diagnostic small, aiding shielding and deflection of any charged particles away from the entrance aperture. The optical light emitted is imaged, and the energy deposited in the scintillators can be measured.

II. DESIGN

A schematic of the diagnostic is shown in Fig. 1. The scintillators are housed in an aluminum casing that provides collimation and shielding. The x-rays enter through one end of the housing, allowing the x-rays to pass through

a)Electronic mail: dean.rusby@stfc.ac.uk

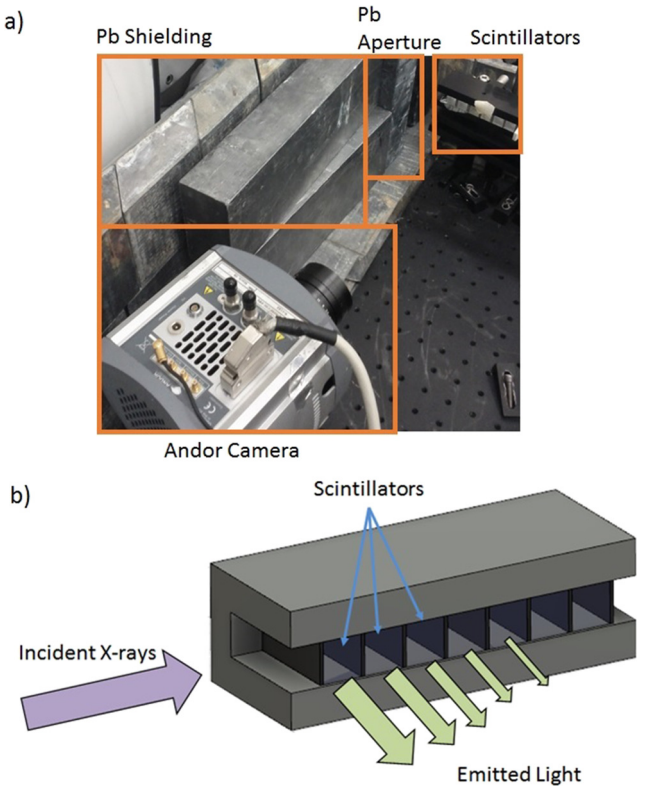

FIG. 1. (a) The diagnostic in a typical experimental setup with the camera, aperture, and typical lead shielding. (b) A computer aided design (CAD) drawing of the diagnostic. The x-rays enter an array of scintillators encased in aluminum and are attenuated as they pass through. The scintillators will emit light that is captured using a camera. The scintillators are wrapped in PTFE and optically separated using thin Al foil in order to prevent light produced from one layer crossing into another.

scintillators sequentially, one after another. The light emitted from the scintillators escapes through the open side of the detector and is captured on a camera. The scintillators themselves are wrapped in white polytetrafluoroethylene (PTFE) tape and aluminum foil. The PTFE tape ensures that any light that does not come straight out of the scintillator is reflected along the edges and provides uniformity, whereas the Al foil does not. However, Al foil is also necessary to optically separate each layer from one another. We present two designs that are used to measure two different sources of x-rays from laser plasma interactions, as well as a method of optimising the scintillator design for the particular spectral range from a given source.

A. Solid target bremsstrahlung characterisation

To test the capabilities of this spectrometer, it was deployed on a solid target experiment at the Vulcan laser,[2] a Nd:YAG laser operating at a wavelength of 1 μm. The achievable beam energy onto a variety of targets was between 130 and 140 J with a pulse duration of (10 ± 2) ps. The contrast on the Vulcan laser is approximately 10^7 at 4 ns. The beam was focused to a spot of diameter 7 μm FWHM. The peak achievable intensity is therefore $\sim 1 \times 10^{19}$ W/cm^2. From the given scaling laws[15–17] relating intensity of the laser to the hot-electron temperature, the hot-electron temperature for this interaction is estimated to be between 500 and 1000 keV. The x-rays emitted as these electrons pass through the target are expected to have similar energies.

The chosen scintillator to characterise the x-rays emitted from the target was Bismuth Germinate (BGO), which is a dense (7.13 g/cm^3), high Z crystal with high attenuation and light output (8000 photons/MeV). The scintillator is $12 \times 30 \times 2$ mm, where the thickness in the attenuation direction is 2 mm. The primary decay time is measured to be 300 ns. If we allow 10 μs between shots to enable the scintillator to fully decay and no accumulation of light between shots to occur, this scintillator could operate up to 0.1 MHz. The camera used to capture the emitted light is an Andor Neo CMOS, which is a 16-bit camera capable of operating at 100 frames/s for full frame images. Therefore, the maximum repetition rate of this system is currently 100 Hz.

To calculate the response of an absorption spectrometer, the NIST XCOM[18] attenuation tables can be used initially. However these tables neglect that any scattered x-rays could be later absorbed in the scintillator, which will occur predominantly at energies greater than 100 keV. Therefore, a more accurate method is needed for the final design. The Monte Carlo code GEANT4 is used to generate an accurate simulation of the absorbed energy in the scintillator layers. The absorbed fraction of x-ray energy as a function of incident energy is shown in Fig. 2. As the scintillator is thin, it is spaced out with 12 mm of plastic to ensure that the light emitted from each crystal does not transfer into one another and to reduce the amount of x-ray scattering between layers. An example of the raw data taken on the spectrometer is shown in Fig. 3. A number of raw data shots are shown in Fig. 4 with 3 shots of similar incident laser energy and a fourth lower energy to demonstrate the shot-to-shot variation of x-rays from a laser-solid target interaction.

The x-ray spectrum from a solid-target laser-plasma interaction depends on the internal hot-electron temperature. To extract the temperature, the experimental output is compared to simulated x-ray spectra from GEANT4 for different

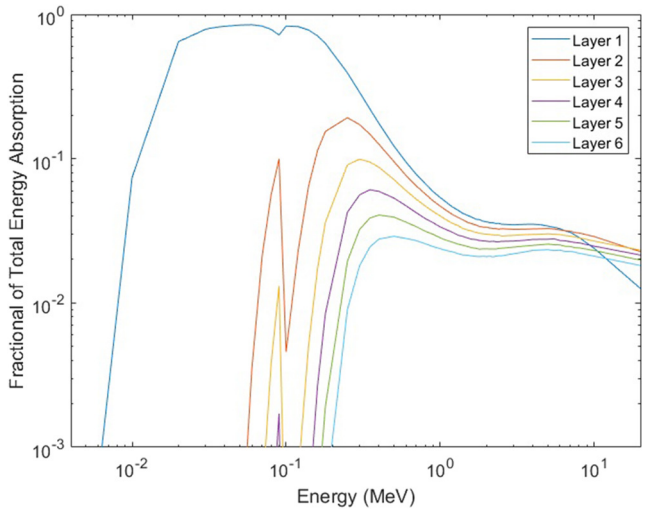

FIG. 2. The fractional absorption of layers of 2 mm thick BGO interlaced with plastic to separate the energy response produced from GEANT4 simulations.

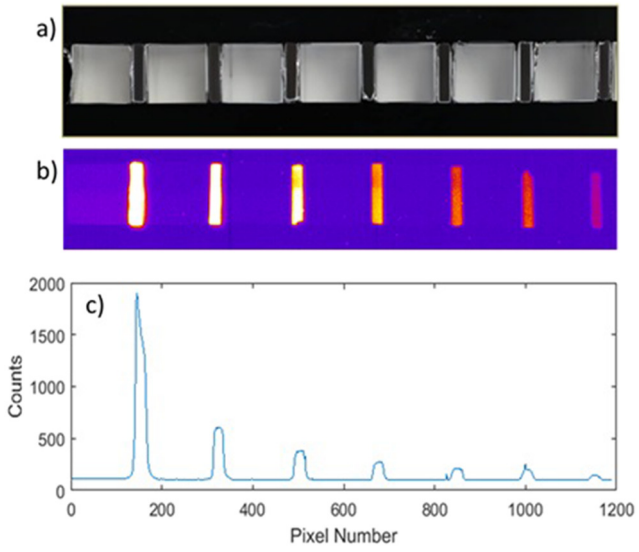

FIG. 3. Example output of the scintillator diagnostic from a shot with 127 J on target. (a) An illuminated image of the scintillator array prior to the shot. (b) An example measurement taken on the spectrometer and (c) the lineout of the image showing a decrease in the emitted light as a function of layer.

Maxwellian electron spectra. The temperature is varied until the variance is minimised as determined by the least-squares method. To take into account the uncertainties of the data, the comparison is repeated many times and each time the comparison is done, the uncertainties are added to the data randomly according to a normal distribution yielding many temperature fits which are then plotted in a histogram; an example of which is shown in Fig. 5. The uncertainties in the data are estimated as the standard deviation in the measurement and the known single shot pixel error that arises from noise within the camera system. The average is taken as the resulting temperature of that shot and the standard deviation of the histogram is used as the uncertainty in the temperature extraction. The normalised mean

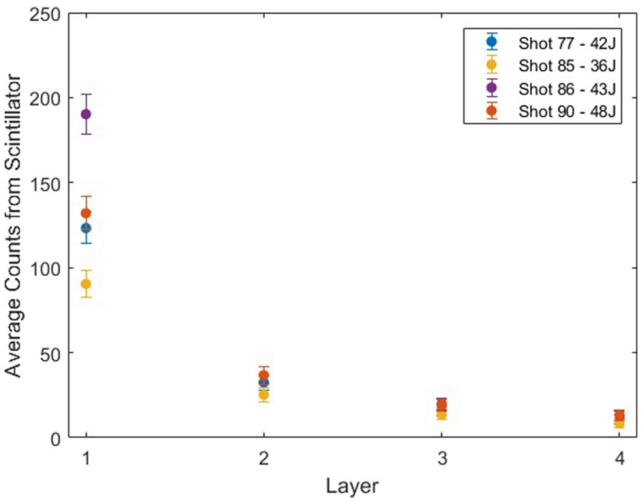

FIG. 4. Example outputs from the diagnostic for 3 shots with similar energies and a shot with lower energy.

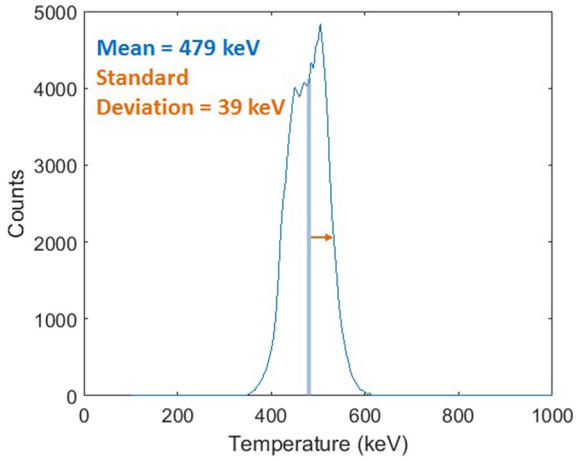

FIG. 5. A histogram of the fitted temperatures from a simple measurement by comparing the predicted output of the diagnostic for different simulated x-ray spectra multiple times. Each time errors from the experimental data are randomly added. The mean is taken as the temperature of the data, and the standard deviation from this mean is the error in the temperature measurement.

counts are shown in Fig. 6 with a predicted output using a temperature fit.

B. Betatron spectrometer characterisation

The second spectrum that was chosen to test the capabilities of the diagnostic was a betatron source. Betatron x-rays arise from electrons oscillating transversely during laser wakefield acceleration[19,20] and peak at lower energies (<80 keV) in comparison to bremsstrahlung x-rays from solid target interactions. It will therefore require a different arrangement of scintillators to properly characterise these lower energy x-rays. EJ-208, a plastic scintillator, was chosen as it has a lower density (1.023 g/cm^3) than BGO and a higher light yield (9200 photons/1 MeV electron). It has a decay time of 3.3 ns, which is much shorter than BGO. The arrays were imaged using an Andor Neo CMOS camera, as before; this again limits the system to 100 Hz. Each scintillator is cut to the size of

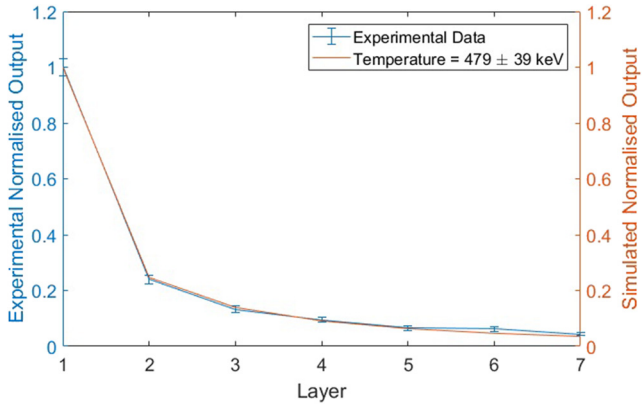

FIG. 6. An example measurement taken from the spectrometer that has been normalised to the first layer. The simulated output of the diagnostic for a simulated spectrum is also plotted, where the temperature for this spectrum is (479 ± 39) keV.

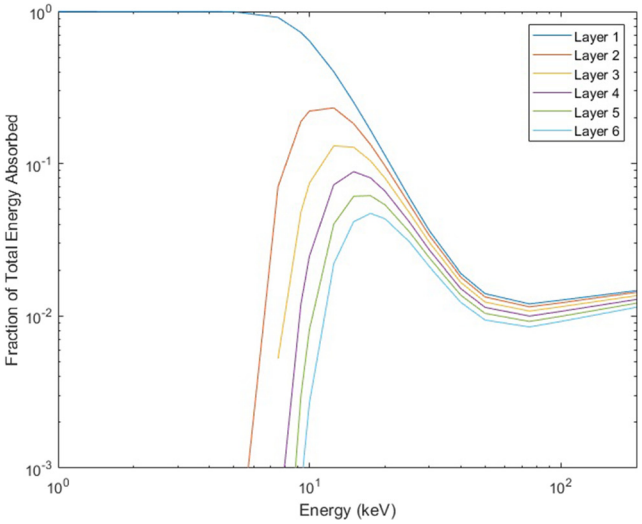

FIG. 7. Fractional absorption of 5 mm of EJ-208 produced from GEANT4 simulations.

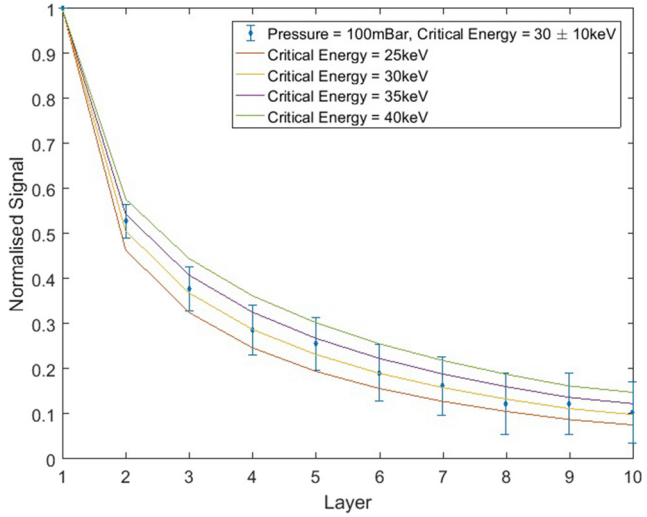

FIG. 8. A measurement of the betatron spectrum taken using the spectrometer that is normalised to the output of the first layer. The predicted outputs of the diagnostic for a number of different critical energies are also plotted using Eq. (1), and the response function is shown in Fig. 7. The critical energy for the data recorded from this shot is (30 ± 10) keV.

$12 \times 30 \times 5$ mm, where 5 mm is the thickness of the scintillator in the attenuation direction. The deposited energy as a function of x-ray energy of the design created from GEANT4 simulations is shown in Fig. 7.

The intensity of a betatron angular spectrum[20,21] is given as

$$\frac{d^2 I_B}{d\Omega d\theta_B} = \frac{\gamma^2 \xi_B^2}{1+\gamma^2\theta_B^2}\left[K_{2/3}^2(\xi_B) + \frac{\gamma^2\xi^2}{1+\gamma^2\theta_B^2}K_{1/3}^2(\xi_B)\right], \quad (1)$$

where θ_B is the angle away from the axis and $K_{2/3}^2$ and $K_{1/3}^2$ are modified Bessel functions. $\xi_B = (E/E_c)(1+\gamma^2\theta^2)^{3/2}$, where E_c is the critical energy, which is described as the point at which half the energy is above and below.

The betatron x-rays were created during an experiment on the Astra-Gemini laser, which delivered up to 15 J of 800 nm radiation with a pulse length of 45 fs.[22] The beam was focused using an F-40 parabola onto a gas cell with an elliptical focal spot size of (43 ± 9) μm by (39 ± 8) μm. The laser is capable of firing once every 20 s. A gas cell is used to control the length and density of the gas used in the interaction. All the high-energy electrons generated during the laser plasma interactions are deflected using a 40 cm 0.9 T magnet. The betatron x-rays exit the vacuum chamber through a 250 μm thick Kapton window to minimise attenuation. The x-rays are then recorded on the scintillator-based spectrometer. The spectrometer is housed inside 50 mm of lead in all directions, with an open aperture at the front. Additional scintillators are placed inside the lead to monitor any harder x-rays that penetrate the shielding.

The data shown in Fig. 8 were measured on a shot taken at 100 mbar plotted with error bars from the uncertainties discussed above. The expected outputs of the data from multiplying the spectrum calculated from Eq. (1) by the response curves from GEANT4, as shown in Fig. 7 are also plotted in Fig. 8. The comparison between the data and expected values is conducted similar to the solid target example. For the data shown in Fig. 8, the critical energy is found to be (30 ± 10) keV. The large error bars are the result of the low brightness of the betatron signal.

III. ABSOLUTE CALIBRATION

As we are aware, the collection of the light emitted by the scintillators will vary depending on the camera, lens, and experimental setup. Therefore, each setup needs to be calibrated using a known source. In this section, we have used the hard x-ray spectrometer, primarily due to the x-ray sources available, and a radioactive source to first confirm the diagnostic performance as a spectrometer and second calculate the counts on the camera per unit of x-ray energy absorbed in the scintillators. This can then be related to the number of x-rays depending on the determined temperature of the spectrum.

The radiation sources used in this calibration were an isotropic Sodium-22 (Na-22) and a Cobalt-60 (Co-60). The Na-22 source emits a beta-plus, that annihilates into two 511 keV gammas, and also a 1.275 MeV gamma. The branching ratio of these two is approximately 91% and 9%, respectively. The activity of the source at the time of measuring was approximately 166 kBq. The Co-60 source emits either a 0.31 MeV beta or a 1.48 MeV beta, with a branching ratio of 99.88% and 0.12%, respectively. This cause the Co-60 to decay into a metastable state of Ni-60 which decays emitting two gammas, 1.173 MeV and 1.332 MeV. The ratios of these two x-rays are 53% and 47%, respectively. The emitted beta from each of these sources will be absorbed by the air and the plastic layer that is before the first layer of BGO.

As the x-ray output of the Na-22 source was quite low compared to a laser-plasma interaction, the camera used to image the scintillator array needed to integrate for a long period of time. In this case 20 min per integration, the camera and lens were the same used in the high-energy bremsstrahlung

experiment described earlier; an Andor Neo CMOS in the same configuration as in that experiment. To improve the signal to noise, 45 images were added together, and also a 10 cm Pb brick was placed in-between the camera and the source to reduce the direct x-rays from the source. Due to the long integration, the entire setup needed to be enclosed in a light tight box; tests were done to conclude that the light tightening was suitable for the 20 min of integration. Also the camera was cooled to the maximum achievable without water cooling, −40 °C. The same procedure is repeated for the Co-60 source.

The source was placed 56 mm from the first BGO layer of the high-energy design discussed early. Assuming a perfectly 4π emission of x-rays, the solid angle that each scintillator occupies could be calculated. However, due to additional effects, such as scattering of the x-rays off the Al cladding, GEANT4 simulations were conducted to provide the most precise estimation of the energy absorption from each emission line of each of the sources. The Al cladding was included in the GEANT4 simulations as the scattering from the 4π source will have a large effect.

The normalised results for the output of the high energy scintillator array for both sources are shown in Fig. 9. The uncertainty is measured as the standard deviation of the array of the crystal analysed. Also plotted is the simulated output using GEANT4. The two sets of experimental data match very closely with the predicted values. From this, we can conclude that the spectrometer behaves as predicted. After layer 3, the light output of the layers is low and the uncertainities are very high. The same measurement using just the Co-60 source was conducted using the scintillator array for betatrons. The results, shown in Fig. 10, are normalised to the second layer as the emitted electrons are absorbed in the first layer. The results from the measurement match with the simulations from GEANT4.

As we know the activity of the source, we can estimate the number of x-rays and the energy absorbed in the 20 min integration time. From the average number of counts in each layer, we can estimate the counts per MeV deposited. This is shown in Fig. 11 as a function of layer number for the two sources. This shows that there is approximately 1 count for every 1750 MeV absorbed for the first layers.

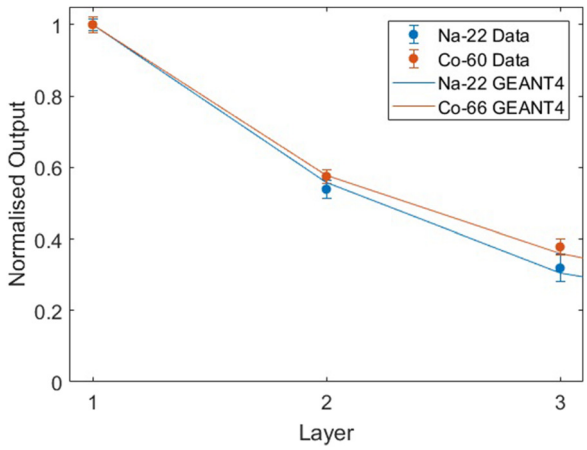

FIG. 9. Calibration of the diagnostic conducted using a Na-22 and Co-60 source. The data match well with the predicted data from GEANT4 for the two calibration sources. After layer 3, the data become difficult to detect due to the low activity of the source despite the long acquisition time.

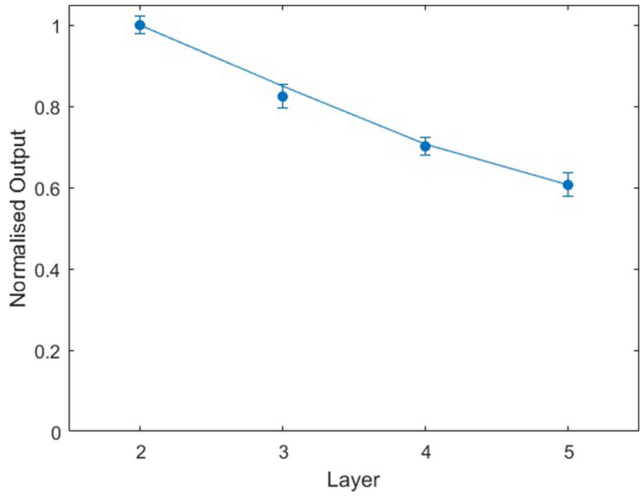

FIG. 10. The calibration of the betatron scintillator array using the Co-60. The data are normalised to layer 2 to ensure that it is only the x-ray absorption and not the electrons emitted from the source.

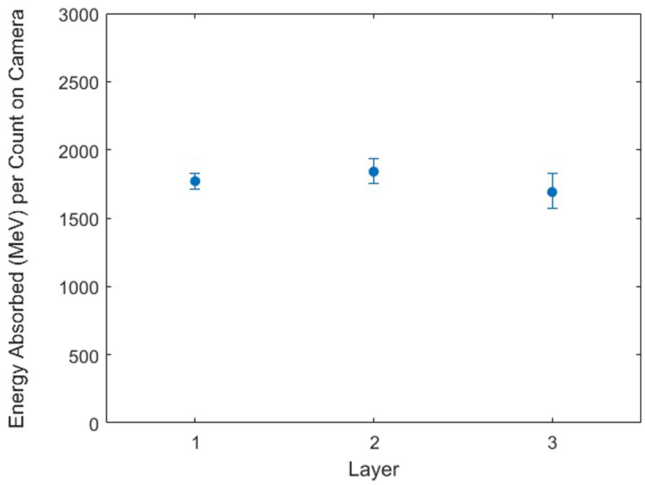

FIG. 11. The amount of energy required to measure a single count on the camera as a function of layer. The result is consistent for the first three layers.

IV. SCINTILLATOR OPTIMISATION

We have demonstrated the use of the scintillator diagnostic to characterise X-ray generation in two different types of x-ray sources that range from tens of keV to hundreds of keV. The main changes that allow the scintillator to be optimum for the sources shown here were the composition, layer thickness, number of layers, and density of the scintillator. As most of these parameters are fixed for a particular scintillator, a systematic optimisation can be performed by varying the scintillator thickness until the output is ideal for a chosen x-ray spectral range. To create the ideal spectrometer for a particular type

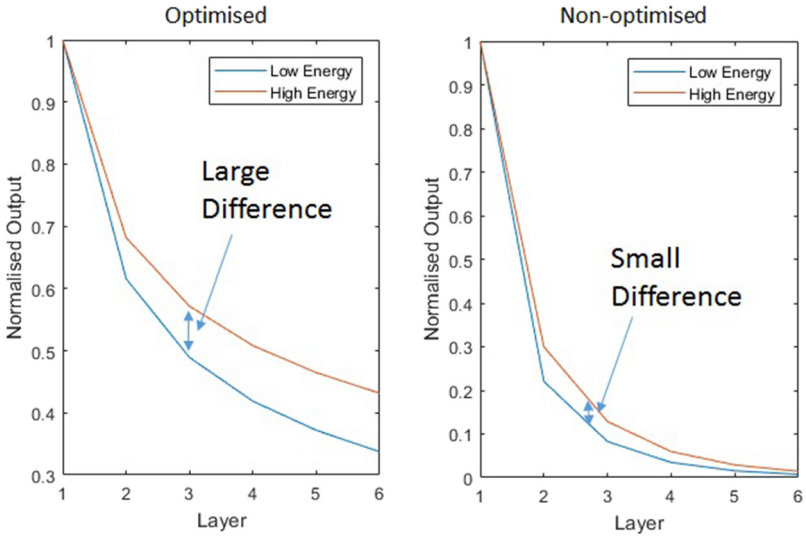

FIG. 12. An example of an optimised thickness of scintillator for an arbitrary high and low energy x-ray source. For the optimised thickness, the scintillator output will have a larger difference between the energy ranges of interest. For the non-optimal thickness, the scintillator will have a small difference.

of x-ray radiation, we must have the largest change in output in the spectral region of interest. An example of this is shown in Fig. 12 for an arbitrary high and low energy x-ray source and scintillator thickness. The large difference indicates that the scintillator thickness has been optimised. When the scintillator thickness is non-optimal, the difference will be small.

To demonstrate this technique, we again choose the betatron source and the EJ-208 scintillator. To find the ideal thickness of the scintillator for a betatron source with a critical energy between 10 and 20 keV, we find the ideal outputs of the spectrometer with 5 layers for these energies.

Figure 13(a) shows the differences between the scintillator outputs for the two different spectrum inputs when the signal is normalised to the first layer. The optimum thickness of each layer decreases as the signal goes further into the stack. The optimum scintillator thickness would obviously keep decreasing as more scintillators are introduced. However, the brightness of the scintillator signal is of importance to reduce the uncertainties, as shown by the previous characterisation. Therefore, not reducing the thickness too much will ensure that the signal is bright enough to perform the best characterisation but also keeping the scintillators thick enough such that there are enough layers to sample from. The optimum thickness is therefore found by taking the average of all the outputs of all the layers, as shown in Fig. 13(b). This design optimises for a scintillator layer thicknesses of approximately 0.25 cm.

This process has also been repeated for typical bremsstrahlung spectra from a solid target. The spectral range is chosen to be between temperatures of 200 and 800 keV, with the chosen scintillator as 8 layers of BGO. The results of the optimisation are shown in Fig. 14. The optimum thickness for this case is 0.2 cm.

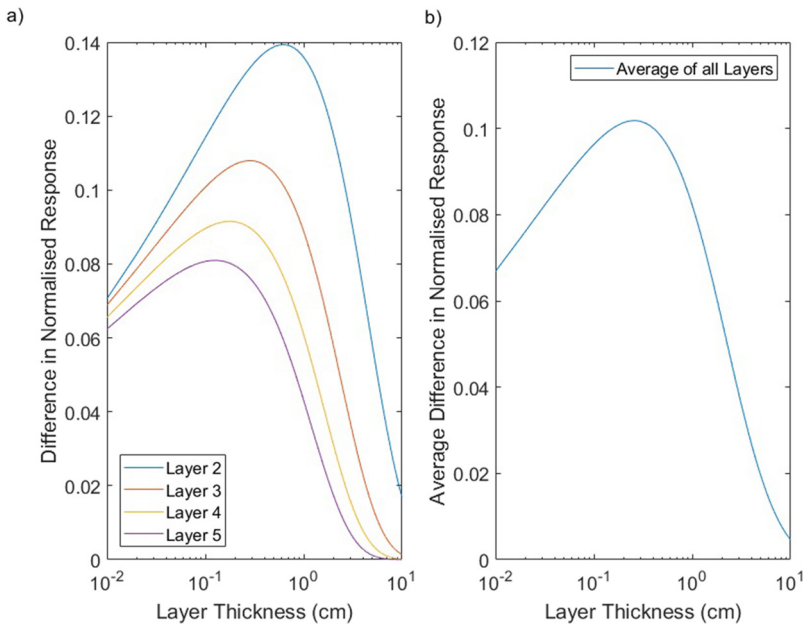

FIG. 13. (a) The difference between the output of each layer of EJ232 using input betatron spectra with critical energies of 10 and 20 keV. The optimum is found when these differences maximise. (b) The average of these outputs is used to determine the optimum thickness for this spectral range.

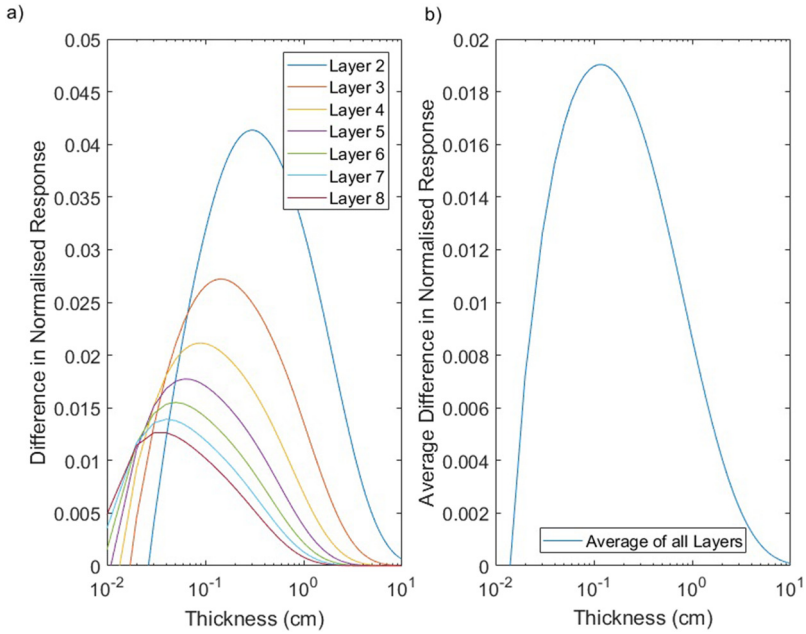

FIG. 14. (a) The difference between the output of each layer of BGO using an input bremsstrahlung spectra from electron temperatures of 200 and 800 keV propagating through a 100 μm Cu target. The average of these is shown in (b).

V. CONCLUSIONS

We have demonstrated the use of an absorption-based x-ray spectrometer with scintillators as both the filter and active material. We have deployed two designs on different experiments to characterise the x-ray radiation from two vastly different sources from laser-plasma interactions. This demonstrates the versatility of the diagnostic to be used on different x-ray sources. These characterisations were also conducted on different laser systems; in particular, the Astra-Gemini laser is capable of firing once every 20 s. This demonstrates the ease of using such a scintillator design on relatively high repetition rate systems. Whilst the decay time of the scintillators used should allow it to operate on much higher repetition rate systems, the limiting factor during these runs would have been the camera system that was only capable of operating at 100 frames/s. For future campaigns where higher repetition rates may be available, the camera could easily be exchanged for one which is much faster.

We have also shown the ease of designing the diagnostic to be optimised for different spectral regions by running through the outputs of the spectrometer for many thicknesses of layers and known spectra. We show two examples, first using EJ-208 and a betatron spectrum with the spectral region of interest between critical energies of 10 and 20 keV and then using BGO and a bremsstrahlung spectrum from a Cu target between the temperatures of 200 and 800 keV. This technique can readily be used with different spectral shapes and scintillators to determine the optimum setup.

ACKNOWLEDGMENTS

The authors gratefully acknowledge the expert assistance of the VULCAN and Astra-Gemini operations and Engineering teams. We also gratefully acknowledge funding from EPSRC Grant Nos. EP/J003832/1, EP/M018091/1, and EP/K022415/1. Data associated with research published in this paper can be accessed at: https://doi.org/10.5286/edata/708.

[1]R. M. Deas, L. A. Wilson, D. Rusby, A. Alejo, R. Allott, P. P. Black, S. E. Black, M. Borghesi, C. M. Brenner, J. Bryant, R. J. Clarke, J. C. Collier, B. Edwards, P. Foster, J. Greenhalgh, C. Hernandez-Gomez, S. Kar, D. Lockley, R. M. Moss, Z. Najmudin, R. Pattathil, D. Symes, M. D. Whittle, J. C. Wood, P. Mckenna, and D. Neely, "A laser driven pulsed x-ray backscatter technique for enhanced penetrative imaging," J. X-Ray Sci. Technol. **23**(6), 791797 (2015).

[2]C. M. Brenner, S. R. Mirfayzi, D. R. Rusby, C. Armstrong, A. Alejo, L. A. Wilson, R. Clarke, H. Ahmed, N. Butler, D. Haddock, A. Higginson, A. McClymont, C. Murphy, M. Notley, P. Oliver, R. Allott, C. Hernandez-Gomez, S. Kar, P. McKenna, and D. Neely, "Laser-driven x-ray and neutron source development for industrial applications of plasma accelerators," Plasma Phys. Controlled Fusion **58**(1), 014039 (2016).

[3]C. Courtois, R. Edwards, A. C. La Fontaine, C. Aedy, S. Bazzoli, J. L. Bourgade, J. Gazave, J. M. Lagrange, O. Landoas, L. Le Dain, D. Mastrosimone, N. Picho, G. Pien, and C. Stoeckl, "Characterisation of a MeV bremsstrahlung x-ray source produced from a high intensity laser for high areal density object radiography," Phys. Plasmas **20**, 083114 (2013).

[4]J. M. Cole, J. Wood, N. Lopes, K. Poder, J. Bryant, S. Alatabi, D. R. Symes, R. Abel, S. Kneip, S. P. D. Mangles, and Z. Najmudin, "Microtomography of human trabecular bone with a laser-wakefield driven x-ray source," Plasma Phys. Controlled Fusion **58**, 014008 (2014).

[5]R. H. H. Scott, F. Perez, M. J. V. Streeter, E. L. Clark, J. R. Davies, H.-P. Schlenvoigt, J. J. Santos, S. Hulin, K. L. Lancaster, F. Dorchies, C. Fourment, B. Vauzour, A. A. Soloviev, S. D. Baton, S. J. Rose, and P. A. Norreys, "Fast electron beam measurements from relativistically intense, frequency-doubled laser solid interactions," New J. Phys. **15**(9), 093021 (2013).

[6]D. R. Rusby, C. M. Brenner, C. Armstrong, L. A. Wilson, R. Clarke, A. Alejo, H. Ahmed, N. M. H. Butler, D. Haddock, A. Higginson, A. McClymont, S. R. Mirfayzi, C. Murphy, M. Notley, P. Oliver, R. Allott, C. Hernandez-Gomez, S. Kar, P. McKenna, and D. Neely, "Pulsed x-ray imaging of high density objects using a ten picosecond high-intensity laser driver," Proc. SPIE **9992**, 99920E (2016).

[7]C. D. Chen, "Spectrum and conversion efficiency measurements of suprathermal electrons from relativistic laser plasma interactions," Ph.D. thesis, Massachusetts Institute of Technology (MIT), 2009.

[8]C. D. Chen, J. A. King, M. H. Key, K. U. Akli, F. N. Beg, H. Chen, R. R. Freeman, A. Link, A. J. Mackinnon, A. G. MacPhee, P. K. Patel, M. Porkolab, R. B. Stephens, and L. D. Van Woerkom, "Bremsstrahlung

spectrometer using k-edge and differential filters with image plate dosimeters," Rev. Sci. Instrum. **79**(10), 10E305 (2008).
[9]S. Chauvie, S. Guatelli, V. Ivanchenko, F. Longo, A. Mantero, B. Mascialino, P. Nieminen, L. Pandola, S. Parlati, L. Peralta, M. G. Pia, M. Piergentili, P. Rodrigues, S. Saliceti, and A. Trindade, "Geant4 low energy electromagnetic physics," in *IEEE Symposium Conference Record Nuclear Science* (IEEE, 2004), Vol. 3, pp. 1881–1885.
[10]S. Chauvie, S. Guatelli, B. Mascialino, L. Pandola, M. G. Pia, P. Rodrigues, and A. Trindade, "Validation of Geant4 bremsstrahlung models: First results," in *IEEE Nuclear Science Symposium Conference Record* (IEEE, 2006), pp. 1511–1515.
[11]G. A. P. Cirrone, G. Cuttone, F. Di Rosa, L. Pandola, F. Romano, and Q. Zhang, "Validation of the Geant4 electromagnetic photon cross-sections for elements and compounds," Nucl. Instrum. Methods Phys. Res., Sect. A **618**(1-3), 315322 (2010).
[12]R. H. H. Scott, E. L. Clark, F. Perez, M. J. V. Streeter, J. R. Davies, H. P. Schlenvoigt, J. J. Santos, S. Hulin, K. L. Lancaster, S. D. Baton, S. J. Rose, and P. A. Norreys, "Measuring fast electron spectra and laser absorption in relativistic laser-solid interactions using differential bremsstrahlung photon detectors," Rev. Sci. Instrum. **84**(8), 083505 (2013).
[13]M. J. Mead, D. Neely, J. Gauoin, R. Heathcote, and P. Patel, "Electromagnetic pulse generation within a petawatt laser target chamber," Rev. Sci. Instrum. **75**(10 II), 4225–4227 (2004).
[14]D. P. Mason, S. Banerjee, K. Ertel, P. J. Phillips, T. Butcher, J. Smith, M. De Vido, O. Chekhlov, C. Hernandez-Gomez, C. Edwards, and J. Collier, "High energy diode-pumped solid-state laser development at the central laser facility," Proc. SPIE **9893**, 989309 (2016).
[15]S. C. Wilks and W. L. Kruer, "Absorption of ultrashort, ultra-intense laser light by solids and overdense plasmas," IEEE J. Quantum Electron. **33**(11), 1954–1968 (1997).
[16]M. G. Haines, M. S. Wei, F. N. Beg, and R. B. Stephens, "Hot-electron temperature and laser-light absorption in fast ignition," Phys. Rev. Lett. **102**(4), 045008 (2009).
[17]F. N. Beg, A. R. Bell, A. E. Dangor, C. N. Danson, A. P. Fews, M. E. Glinsky, B. A. Hammel, P. Lee, P. A. Norreys, and M. Tatarakis, "A study of picosecond lasersolid interactions up to 10^{19} W/cm^2," Phys. Plasmas **4**(2), 447–457 (1997).
[18]J. M. Berger, J. H. Hubbell, S. M. Seltzer, J. Chang, J. S. Coursey, R. Sukumar, D. S. Zucker, and K. Olsen, "Xcom: Photon cross sections database," NIST Stand. Ref. Database **8**(1), 3587–3597 (1998).
[19]S. Kneip, C. McGuey, J. L. Martins, S. F. Martins, C. Bellei, V. Chvykov, F. Dollar, R. Fonseca, C. Huntington, G. Kalintchenko, A. Maksimchuk, S. P. D. Mangles, T. Matsuoka, S. R. Nagel, C. A. J. Palmer, J. Schreiber, K. Ta Phuoc, A. G. R. Thomas, V. Yanovsky, L. O. Silva, K. Krushelnick, and Z. Najmudin, "Bright spatially coherent synchrotron X-rays from a table-top source," Nat. Phys. **6**(12), 980, 983 (2010).
[20]F. Albert, B. B. Pollock, J. L. Shaw, K. A. Marsh, J. E. Ralph, Y. H. Chen, D. Alessi, A. Pak, C. E. Clayton, S. H. Glenzer, and C. Joshi, "Angular dependence of betatron X-ray spectra from a laser-wakefield accelerator," Phys. Rev. Lett. **111**(23), 235004 (2013).
[21]E. Esarey, B. A. Shadwick, P. Catravas, and W. P. Leemans, "Synchrotron radiation from electron beams in plasma-focusing channels," Phys. Rev. E **65**(5), 056505 (2002).
[22]C. J. Hooker, S. Blake, O. Chekhlov, R. J. Clarke, J. L. Collier, E. J. Divall, K. Ertel, P. S. Foster, S. J. Hawkes, P. Holligan, B. Landowski, B. J. Lester, D. Neely, B. Parry, R. Pattathil, M. Streeter, and B. E. Wyborn, "Commissioning the astra gemini petawatt ti:sapphire laser system," in *Conference on Lasers and Electro-Optics/Quantum Electronics and Laser Science Conference and Photonic Applications Systems Technologies* (Optical Society of America, 2008), p. JThB2.